frontiers in Energy Research

ORIGINAL RESEARCH
published: 09 January 2020
doi: 10.3389/fenrg.2019.00159

Using Biochar and Coal as the Electrode Material for Supercapacitor Applications

Yan Ding, Tao Wang, Duo Dong and Yongsheng Zhang**

Key Laboratory of Condition Monitoring and Control for Power Plant Equipment, Ministry of Education, North China Electric Power University, Beijing, China

Millet straw activated carbon (MAC) and anthracite coal activated carbon (AAC) was prepared by thermal modification with a mass ratio of 5:1 (KOH:C) for supercapacitor (SC). The BET specific surface area of MAC and AAC is 1,264.8 and 1,695.1 m^2/g with the average pore size of 3.018 and 2.170 nm, respectively. In the cyclic voltammetry test, the area of CVs of MAC electrode is obviously larger than that of AAC, especially at 100 and 200 mV/s. The ESR (0.28 Ω) of AAC electrode is more than 6.5 times that of MAC electrode (0.043 Ω) in the EIS test. In the GCD test, the results illustrate each specific capacitance of the activated biochar electrode is larger than AAC electrode. At the current density of 0.2 A/g, the specific capacitance of MAC electrode is 144 F/g, while the AAC electrode is only 85.2 F/g. The MAC electrode also presents a stable cycling performance with 125% after 10,000 cycles at 0.5 A/g which is 11% higher than 114% of AAC and remains 99.5 and 97.4% of coulombic efficiency because of MAC's rich tube structures and fish-scale-like inner surface. These encouraging results all indicate that excellent electrode material for supercapacitors can be obtained by activating cheaper millet straw biochar.

Keywords: biochar, coal, activated carbon, electrode material, supercapacitor

OPEN ACCESS

Edited by:
Baharak Sajjadi,
University of Mississippi, United States

Reviewed by:
Tianyu Liu,
Virginia Tech, United States
Kai Zhu,
Harbin Engineering University, China

****Correspondence:***
Tao Wang
wangtao0420@163.com
Yongsheng Zhang
yszhang@ncepu.edu.cn

Specialty section:
This article was submitted to Bioenergy and Biofuels, a section of the journal Frontiers in Energy Research

Received: *02 September 2019*
Accepted: *11 December 2019*
Published: *09 January 2020*

Citation:
Ding Y, Wang T, Dong D and Zhang Y (2020) Using Biochar and Coal as the Electrode Material for Supercapacitor Applications. Front. Energy Res. 7:159. doi: 10.3389/fenrg.2019.00159

INTRODUCTION

Under the severe situation of the depletion of non-renewable fossil energy, supercapacitors act as an excellent energy storage device because of the high specific capacitance, high power density, excellent cycle efficiency, and long cycling stability. According to the principle of energy storage, supercapacitors can be divided into electrochemical double layer capacitors (EDLCs) and pseudocapacitors (Pandolfo and Hollenkamp, 2006). The EDLC (Ji et al., 2014) is a kind of energy storage application between the ordinary capacitor and storage battery, and it has higher power density than battery and higher energy density than conventional capacitors. Carbon materials are widely used as electrode materials for supercapacitors in the following aspects: graphene (Yoo et al., 2011; Xu et al., 2013; Naderi et al., 2016), carbon nanotubes (Frackowiak and Béguin, 2002), activated porous carbon (Tian et al., 2015), biochar (Qiu et al., 2018), and carbon aerogels (Saliger et al., 1998). Theses carbon materials show the same advantages of large specific surface area (SSA), stable chemical properties and abundant porosity which are the important factors of supercapacitor materials.

Recent years, there have been considerable efforts made to develop excellent carbon materials for supercapacitors. Zhong-Yu et al. (2018) proposed hierarchical graded porous carbon (1,813 m^2/g) by carbonizing and activating the grapefruit peel with KOH. The specific capacitance of

HPC supercapacitor was 285 F/g at 0.5 A/g in 1 mol/L KOH electrolyte. In Kouchachvili et al. (2015), infested ash tree residues were carbonized at 700°C and activated in dilute HNO_3 with electrochemical properties of a specific capacitance of 470 F/g in 0.75 M H_2SO_4 and 335 F/g in 3 M $LiN(SO_2CF_3)_2$. In Pourhosseini et al. (2018), magnetic biochar with olive-shaped pores and functional biochar with a novel interconnected 3D pore network structure were obtained via the activation with $FeCl_3$ and KOH exhibiting an excellent specific capacitance of 368 F/g and an energy density of 41.5 Wh/kg. Genovese (Genovese and Lian, 2017) used Pine cones as biomass templates to synthesize activated carbon with high SSA (2,450 m^2/g) for the adsorption of redox active polyoxometalate clusters, and the composite has a gravimetric capacitance of 361 F/g. In Subramanian et al. (2007), carbon materials were synthesized from banana fibers treated with $ZnCl_2$ and KOH for the EDLC electrodes, and the SSA of the material was founded to be 1,097 m^2/g with a specific capacitance of 74 F/g in 1 M Na_2SO_4. Besides, there are also many studies on other carbon sources, such as coal (Akash and O'Brien, 2015), coal tar pitch (He et al., 2012) for synthesis of activated carbon. In these articles, there are few papers studied on the preparation of electrode materials from crop biomass for supercapacitors. However, large quantities of crop biomass, such as millet straw, are directly discarded as solid waste, and only a small part is inefficiently used for fertilizer. The biomass waste possesses advantages of universality, richness, renewability and low cost. Therefore, the crop biomass is a kind of good raw materials for activated carbon by a green and sustainable method. Furthermore, coal resources are fine raw materials for activated carbon. Few studies have been carried out to simultaneously study supercapacitors based on the active carbon materials from biomass and coal. Therefore, porous activated carbons were prepared by carbonizing millet straw (millet straw activated carbon, MAC) and anthracite coal (anthracite coal activated carbon, AAC) followed by the KOH activation for active materials of supercapacitors in this work.

This paper aims to systematically analyze the probability of materials activated from millet straw and anthracite carbon in the same experimental conditions. Models of Brunauer-Emmett-Teller (BET), Horvath-Kawazoe (HK), and Barrett-Joyner-Halenda (BJH) were conducted to characterize the activated carbon. The cyclic voltammograms (CVs), electrochemical impedance spectroscopy (EIS), and galvanostatic charge-discharge (GCD) tests were conducted to study the electrochemical characteristics of supercapacitors based on the MAC and AAC. Both MAC and AAC exhibit remarkable physical properties with a SSA up to 1,264.8 and 1,695.1 m^2/g and an average pore diameter of 3.018 and 2.169 nm, respectively. They also display great electrochemical performance with an equivalent series resistance (ESR) of 0.04 and 0.28 Ω and a specific capacitance of 144 and 85.2 F/g at 0.2 A/g in an electrolyte of 2 M KOH. Moreover, the prepared EDLCs with the active materials of MAC and AAC present good cycle stability with retention rates of 87 and 71% after 5,000 cycles at 0.5 A/g. This work provides a tremendous potential methodology for the supercapacitor application in energy storage devices and important support for other researchers to study supercapacitors. The data, findings and recommendations of this paper could provide practical guidance for other researchers.

EXPERIMENTAL

Mechanism of Energy Storage of Supercapacitors and KOH Activation

The electric charge is stored in the double-layer formed between the interface of electrodes and the electrolyte for the EDLCs, and there is no chemical reaction during the whole process of charge and discharge (Grahame, 1947). Pseudocapacitance relates to the potential of electrodes produced by the highly reversible chemical adsorption, desorption and redox reaction of the electroactive substances in the two-dimensional plane of the electrodes or quasi-two-dimensional space of electrolyte's bulk. As known, the capacitance depends on the area, distance and dielectric constant of the two capacitor plates given by

$$C=\frac{\varepsilon A}{d}=\frac{\varepsilon_r \varepsilon_0 A}{d} \quad (1)$$

Where C is the capacitance, A is the surface-area of the electrode, d is the distance of two electrodes, ε is the relative dielectric constant, ε_r is the relative dielectric constant, ε_0 is the vacuum dielectric constant.

Activated carbon has a large SSA (generally more than 1,000 m^2/g), small pore size (>2 nm) and good conductivity. These advantages contribute to an improvement on ε, d, and A. Activated carbon is obtained by activating precursor carbon by means of physical, chemical or catalytic methods. In this work, KOH is used to activate precursor carbon by carbonizing millet straw and anthracite coal. Chemical activation of KOH has many intrinsic advantages and it was widely reported that activated carbon with well-developed microporous structure could be obtained by KOH activation (Yamashita and Ouchi, 1982; Lozano-Castelló et al., 2007).

The widely accepted mechanism of reaction of KOH with carbon includes two steps which are a solid-solid reaction and followed by a solid-liquid reaction. Four key temperature points during KOH activation were put forward in the reference (Wang and Kaskel, 2012) which indicate that the important product of K_2CO_3 forms in reaction at about 400°C as shown in Equation (2), KOH completely reacts at about 600°C, K_2CO_3 decomposes into CO_2 and K_2O and metallic K forms at 700°C in Equation (4) and (5), and pyrolysis of K_2CO_3 is finished at ∼800°C. At higher temperature, C could reacts with CO_2 in Equation (6). Based on the conclusions of Equation (2–6), and the activated carbon has a better supercapacitor performance at 800°C in the reference (Guo et al., 2019), so the temperature of KOH activation in this experiment was set at 800°C.

$$6KOH + 2C \xrightarrow{400^\circ C\ 600^\circ C} 2K + 3H_2 + 2K_2CO_3 \quad (2)$$

$$K_2CO_3 \xrightarrow{700^\circ C\ 800^\circ C} K_2O + CO_2 \quad (3)$$

$$K_2CO_3 + 2C \xrightarrow{700^\circ C} 2K + 3CO \quad (4)$$

$$K_2O + C \xrightarrow{700^\circ C} 2K + 3CO \quad (5)$$

$$CO_2 + C \xrightarrow{800^\circ C} CO \quad (6)$$

Preparation of Millet Straw Activated Carbon and Anthracite Coal Activated Carbon

Preparation process of MAC and AAC was described in **Figure 1**. The millet straw in this experiment was collected from Shaanxi Province, China. Firstly, the millet straw was crushed into powder, then dried in a vacuum oven at 100°C for 24 h and sealed for reserve. Then the dry millet straw powder was washed and filtered three times with deionized water. The filtered biochar solid was placed in a ventilated drier at 110°C for 24 h. The dehydrated powder was packed and compacted in a crucible, and then placed in a tubular furnace with the gas medium of N_2. The temperature of tubular furnace was slowly raised to 800°C as an increasing rate of 8 °C/min and carbonized for 3 h. And then the tubular furnace was cooled down to room temperature at the same decreasing rate. After carbonization, the relative mass of biochar was greatly reduced. The biochar was cleaned with 5 M HCl for 0.5 h to remove insoluble salt followed by being dried for 12 h. After that, the solution of KOH was mixed with biochar at the mass ratio of 5:1 (KOH: biochar). The slurry was magnetically stirred for 12 h, and dried at 100°C for 24 h. The mixed product was put into the tubular furnace for activation at 800°C in a nitrogen atmosphere again. After that, activated biochar was mixed with 2.5 M HCl for several times until pH = 7 to remove the unreacted KOH, then filtered and dried to obtain the activated carbon. The coal is extracted from anthracite in Inner Mongolia, China. It was dealt with the same carbonizing and activating process as MAC. Finally, anthracite activated carbon was prepared.

Electrode Preparation

The working electrode of three-electrode system was prepared with MAC or AAC (80 wt.%) as active materials, polyvinylidene fluoride (PVDF, 10 wt.%) as the binder and carbon black (10 wt.%) as the conducting agent. The three kinds of powder were fully mixed in an agate mortar for 30 min and then mixed with NMP solvent until it became viscous. The resulting slurry was

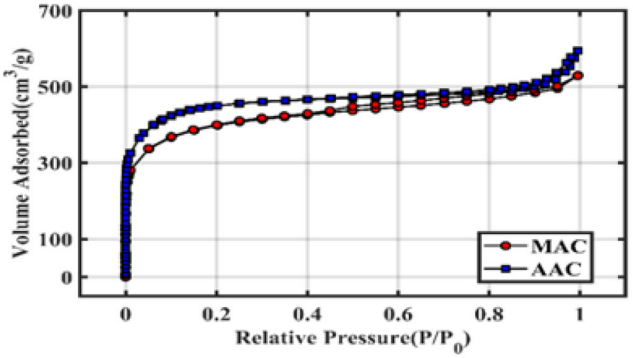

FIGURE 2 | Nitrogen adsorption-desorption isotherm curve for MAC and AAC.

TABLE 1 | Textural properties of MAC and AAC obtained from BET, HK, and BJH model*.

Sample	S_{BET} (m^2/g)	V_{total} (cm^3/g)	V_{mi} (cm^3/g)	V_{me} (cm^3/g)	D_{ap} (nm)
MAC	1,264.8	0.954	0.661	0.293	3.018
AAC	1,424.1	0.907	0.517	0.390	2.169

**SSA was calculated by the BET model based on the adsorption data from 0.01 to 0.1 in the relative pressure (P/P_0); V_{total}, total pore volume; V_{mi}, volume of micropores; V_{me}, volume of mesopores; D_{ap}, adsorption average pore diameter.*

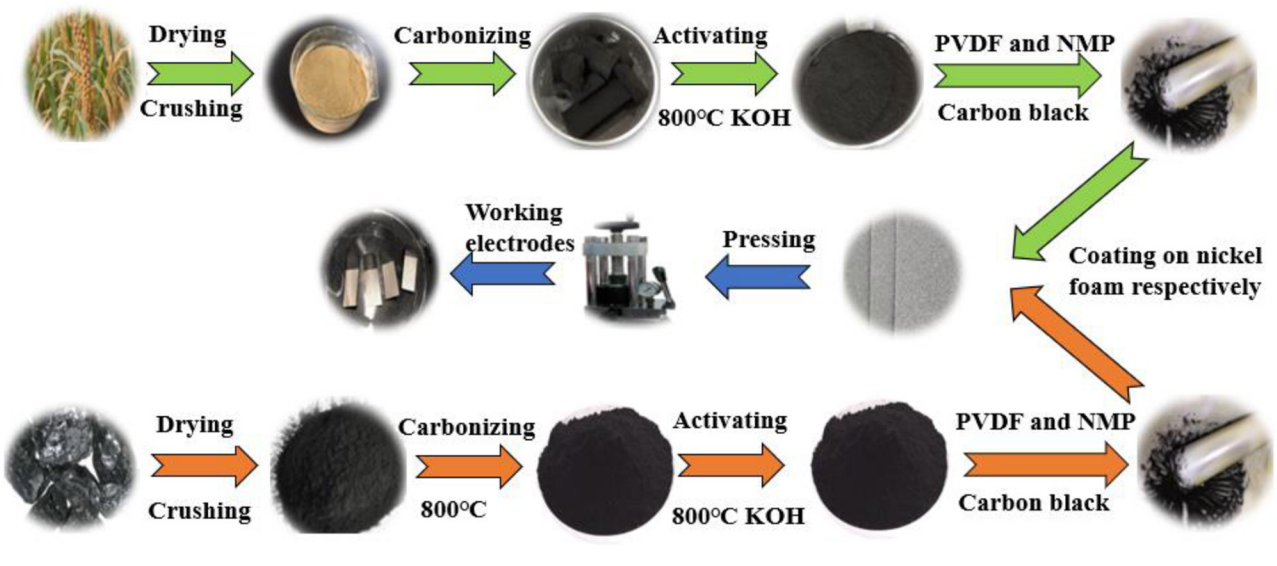

FIGURE 1 | Preparation of modified activated carbon electrode.

coated on the nickel foam current collectors with a square area of 1 cm^2 (1 × 1 cm) and dried in a vacuum drier at 100 °C overnight. The work area was pressed under 8 MPa. The mass loading of AAC electrodes is 2.3 mg with active substrate of 1.84 mg and the mass loading of MAC is 2.2 mg with active substrate of 1.76 mg. After that, working electrodes were soaked in the 2 M KOH solution for 12 h before the electrochemical experiment. The working electrodes were tested in the three-electrode system with a counter electrode of Hg/HgO, a reference electrode of Pt and the electrolyte of 2 M KOH solution. The whole process is also described in the in **Figure 1**.

Testing Methods and Parameters of MAC and AAC

The BET surface and porosity of MAC and AAC were investigated by a Quantachrome Autosorb iQ Station with the nitrogen adsorption at 77 K. The SSA of two kinds of activated carbon was calculated by BET model based on the adsorption data from 0.01 to 0.1 in the relative pressure (P/P_0). The pore size distribution was calculated by HK model for micropore and BJH model for mesopore. The pore volume and average pore diameter were also analyzed. The HITACHI SU8010 emission scanning electron microscopy (SEM) was also used to observe microstructure of two carbon materials at 5 kV.

The electrochemical evaluation of three-electrode system of two supercapacitors was analyzed by PARSTAT 4000 A electrochemical workstation. The cyclic voltammograms (CVs) were collected at various scan rates of 10, 50, 100, and 200 mV/s, and the potential window is −1–0 V vs. Hg/HgO counter electrode. The electrochemical impedance spectroscopy (EIS) measurements were conducted at the frequency in the range of 0.01–100 kHz at an open potential with the amplitude of 0.5 mV. The galvanostatic charge-discharge (GCD) measurements were performed in various current densities from 0.2 to 2 A/g in the same potential range as CVs. And then, button SCs were fabricated to obtain the cyclic stability by continuous GCD tests at a current density of 0.5 A/g with a potential window of −1–0 V for 10,000 cycles by LANHE CT3001A made in Wuhan of China.

Specific capacitance of supercapacitor can been got in the three-electrode system from the GCD curves by the Equation (7) or the CV curves by the Equation (8). The energy density (E) and power density (P) of supercapacitors are calculated according to Equations (9) and (10) respectively.

$$C = I\Delta t/(m\Delta V) \tag{7}$$

$$C = \frac{\int_{V_1}^{V_2} i(V)dV}{2v(V_2 - V_1)} \tag{8}$$

$$E = \frac{C\Delta V^2}{2 \times 3.6} \tag{9}$$

$$P = \frac{3600E}{\Delta t} \tag{10}$$

In the Equation (7), C is the specific capacitance, I is the discharging current, Δt is the discharging time, m is the is the mass of activated carbons and the ΔV is the potential change of the discharging process. In the Equation (8), i (V) is the current, v is the scan rates, and V_1, V_2 are the lower and upper potential limits. In the Equation (9), C is the specific capacitance, ΔV is the potential change of the discharging process. In the Equation (10), E is the energy density and Δt is the discharge time.

RESULTS AND DISCUSSION

Textural Properties of MAC and AAC

The **Figure 2** shows the adsorption-desorption isotherm curves of MAC and AAC. They shows obvious the characteristic of type IV isothermal adsorption-desorption curve with hysteresis loop. It is obvious that AAC has a higher nitrogen adsorption capacity than MAC. The adsorption curves of MAC and AAC increase rapidly at the lower relative pressure ($P/P_0 < 0.05$), indicating the existence of a large amount of micropores in activated carbons which improve the surface area greatly. The two curves tend to be stable at the relative pressure of $P/P_0 > 0.05$. There is no obvious hysteresis loop appearing in the adsorption-desorption isotherm curve of AAC and MAC which illuminates few mesoporous. The curve of MAC and AAC rises rapidly again at the relative pressure of $P/P_0 > 0.95$, manifesting the open structure in the MAC and AAC.

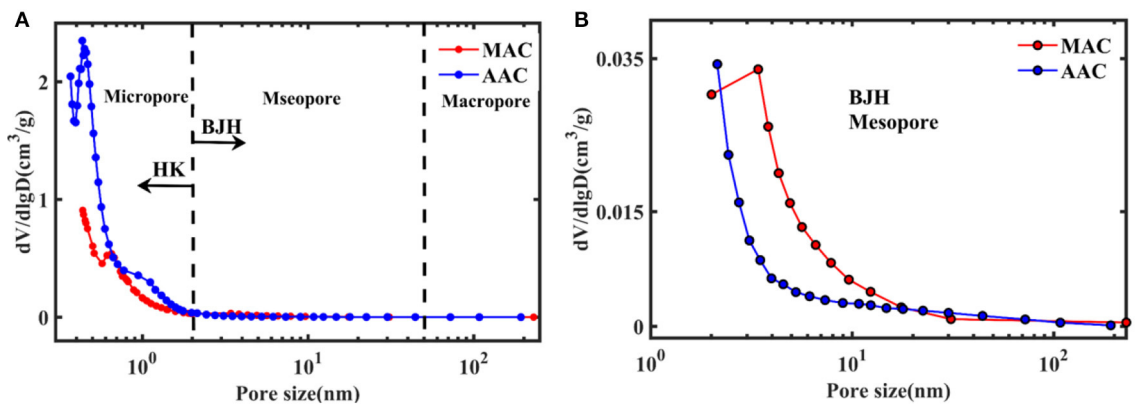

FIGURE 3 | (A) Pore size distributions of MAC and AAC and **(B)** mesopore size distribution in BJH model.

All the above results indicate that MAC and AAC with the activation of KOH are extremely suitable for the active materials of supercapacitors.

The great performance of active carbon electrode materials of supercapacitor mostly rely on the large SSA and high-developed porosity. As shown in the **Table 1**, the BET SSA

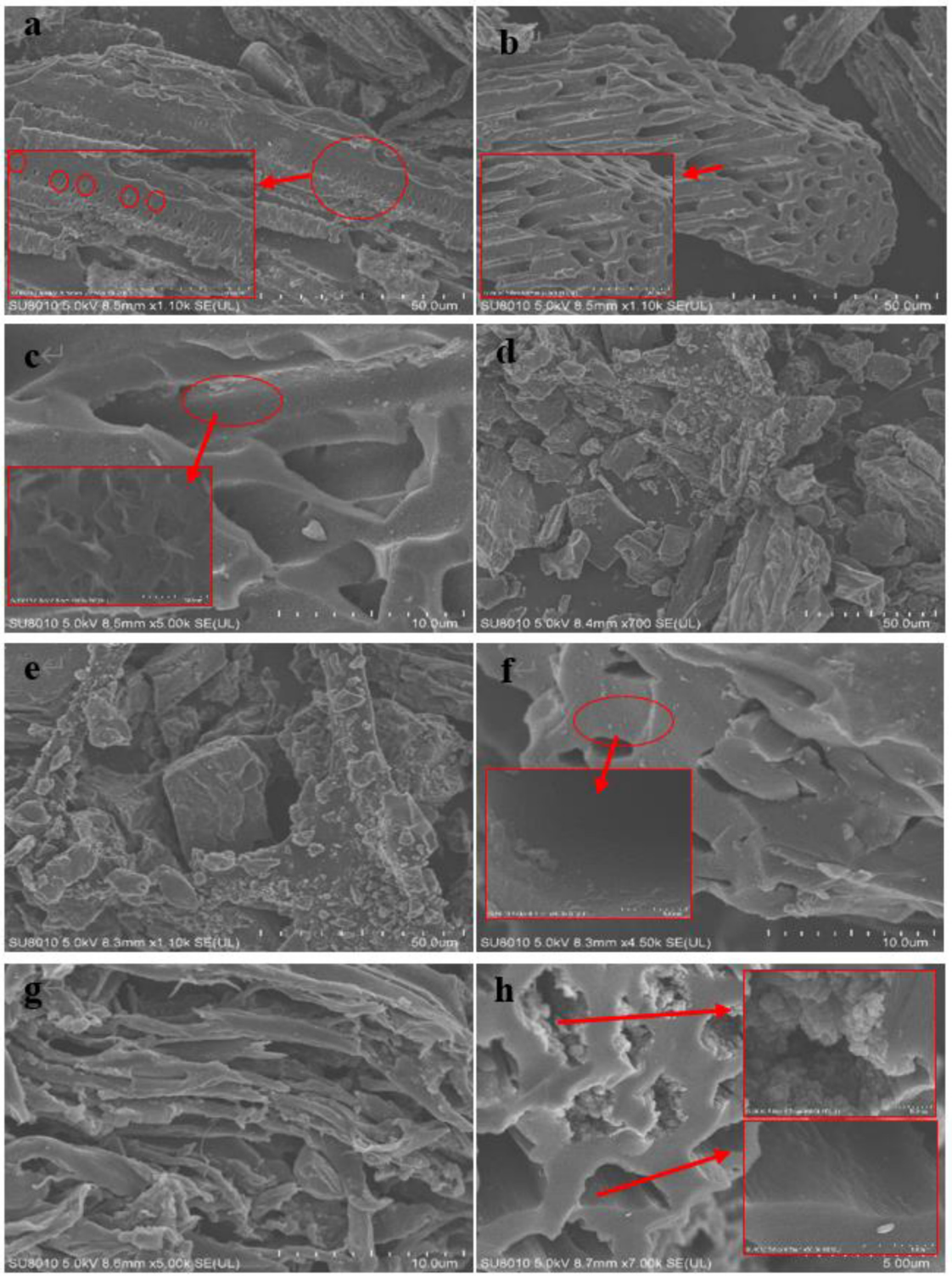

FIGURE 4 | (a–c) are SEM imagines of MAC, **(d–f)** are SEM imagines of AAC, **(g,h)** are SEM imagines of non-activated millet straw carbon.

of MAC (1,264.8m^2/g) is smaller than AAC (1,424.1 m^2/g), but the total pore volume (0.954 cm^3/g) and the mesoporous volume (0.661 cm^3/g) of MAC are higher than AAC (0.907 and 0.517 cm^3/g) which contributes to ions storage in MAC (Liu et al., 2015). The adsorption average pore diameter of MAC is 3.018 nm and also higher than AAC (2.169 nm). All the data illustrates MAC has superior pore diameter and volume data compared with AAC except for SSA, only less 159.3 m^2/g. Therefore MAC could provide more space for the electrolyte ions to accommodate and makes them easier to diffuse in the wider transport pores, improving the adsorbate accessibility for double layer capacitance (Pandolfo and Hollenkamp, 2006).

Figure 3A shows the pore size distribution of MAC and AAC in HK model. The apertures of MAC and AAC mainly distribute in the range of micropore and ultramicropore, which increase the SSA and play a vital role of molecular sieve. It can also see that the specific pore volume of each micropore size of AAC is larger than MAC, especially at less than aperture of 0.667 nm. **Figure 3B** shows mesopore size distribution in BJH model. The mesoporous volume of MAC is generally larger than AAC. What's more, mesopore is of importance for specific capacitance (Pandolfo and Hollenkamp, 2006).

SEM Analysis

In order to show the morphology, SEM was performed. According to images of MAC (**Figures 4a–c**), AAC (**Figures 4d–f**) and non-activated millet straw carbon. it can be clearly seen that there are many elliptical pores on the surface of MAC. MAC also shows strip particles with abundant hollow tube structures on the cross section with a diameter of 1–5 μm which are conducive to the movement of the electrolyte ions and reduce diffusion resistance as shown in **Figure 4b**, and this view is also reported in reference (Dai et al., 2017). However, as shown in **Figures 4d,e**, there is almost no pores on the surface of AAC, and most granules of AAC are smaller blocks which may be the reason why AAC shows larger BET surface, and a few hollow tube structures appear on the section of AAC. MAC tubes show fish-scale-like inner surface presented in the inset image of **Figure 4c** which can provide more space for electrolyte ions so as to improve the specific capacitance. However, the inner surface of AAC tube is smooth which can provide less attachment space for electrolyte ions. On the other hand, the SEM images of millet straw carbon without KOH activation are shown in **Figures 4g,h** which show a strip shape of granules, but there is no pore on the surface. A lot of impurities block up the tube, and some tubes present smooth internal surface. These results indicate that KOH activation

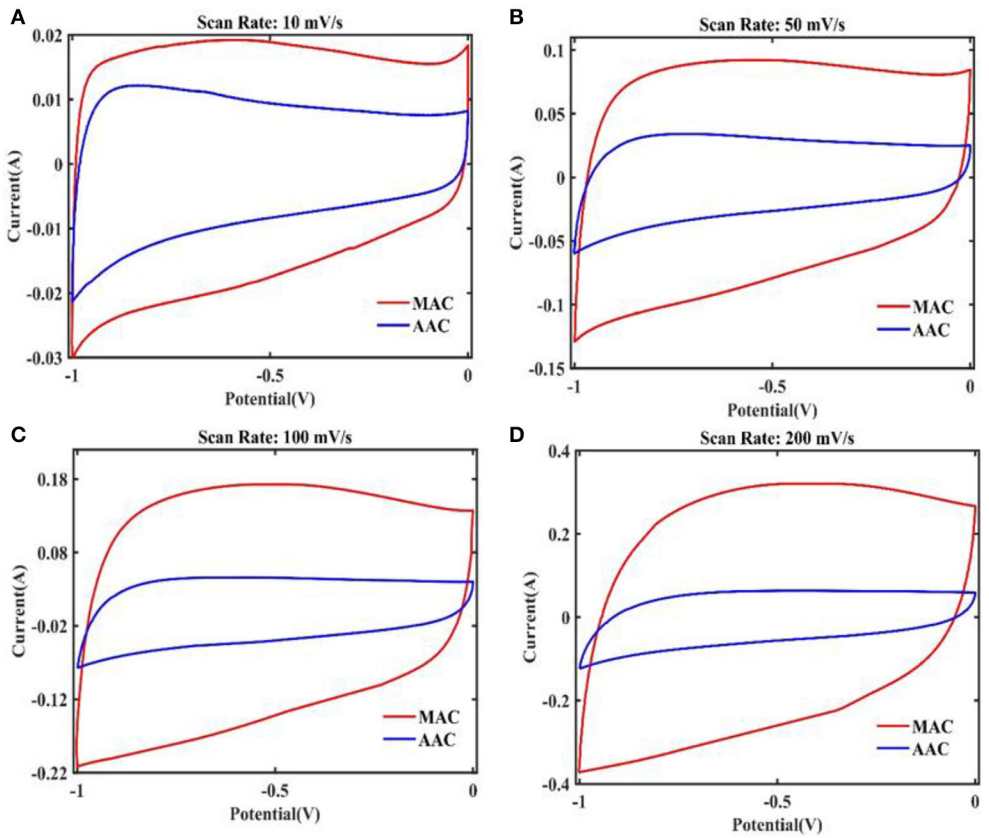

FIGURE 5 | The CV curves of MAC and AAC at the scan rates of **(A)** 10 mV/s, **(B)** 50 mV/s, **(C)** 100 mV/s, and **(D)** 200 mV/s.

increases the pores and surface area, and MAC performs more obviously.

Electrochemical Performance of Supercapacitors of MAC and AAC

In order to study the electrochemical performance of MAC and AAC as electrode active materials for supercapacitors CV, EIS, and GCD tests were carried out in 2 M KOH aqueous through three-electrode system.

CVs Test

Figure 5 shows the CV curves of MAC and AAC at the scan rates of 10, 50, 100, and 200 mV/s. It can be seen that the area surrounded by curve of MAC is larger than AAC at each scan rate, indicating the specific capacitance of MAC as an electrode is larger than AAC at each scan rate. With the same increase of scan rate, the area of CV curves of MAC increases faster, indicating a good performance in the higher scan rate. There is no obvious peaks appear in the MAC and AAC curves at 10, 50, and 100 mV/s, suggesting a no pseudocapacitor performance of electrodes of MAC and AAC (Rose et al., 2011). **Figures 6A,B** show the CV curves of MAC and AAC at four kinds of scan rate in the 3D coordinates, **Figures 6C,D** describe CV curves of AAC and MAC in potential-current plane. It can be seen that all the curves keep better quasi-rectangular shape in the two groups of curves. What's more, CV curves gradually approach to the rectangular shape with the gradual increase of scan rate,

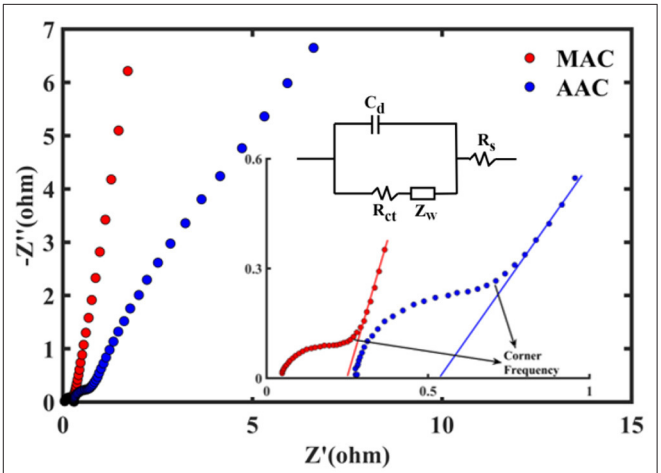

FIGURE 7 | Nyquist plots of the MAC and AAC electrodes in a frequency ranged from 0.01 to 100 kHz and the inset of the high frequency region and corner frequency and the equivalent circuit.

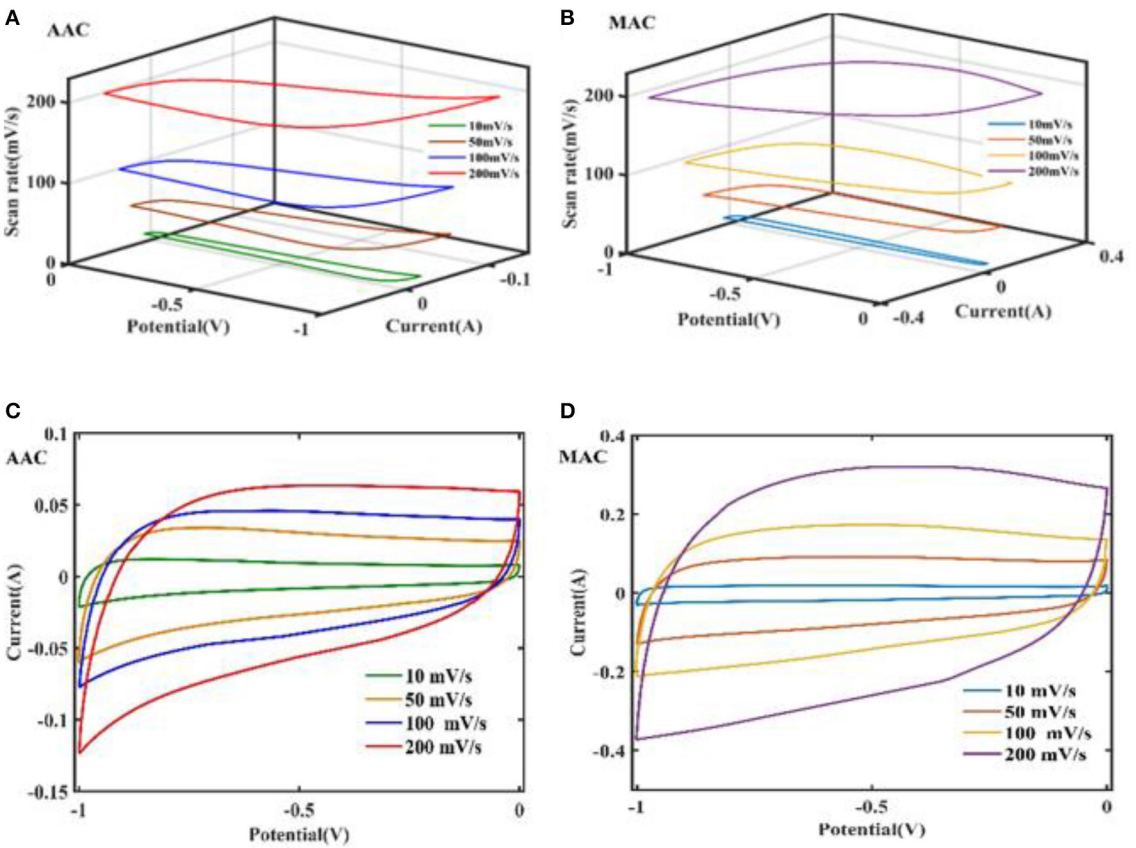

FIGURE 6 | 3D-CVcurves of **(A)** AAC and **(B)** MAC at different scan rates; CV curves of **(C)** AAC and **(D)** MAC in potential-current plane at different rates; CV curves of AAC.

illustrating the capacitance of supercapacitors mainly originates from the EDLC with a good performance and little electrolyte ion diffusion resistance.

EIS Test

In order to determine internal charge-discharge transfer kinetics and electrolyte ion diffusion resistance of AAC and MAC, EIS tests were performed and results are shown in **Figure 7**. The Nyquist plot includes the oblique linear part in low frequency regions and the semicircle portion in high frequency regions, explaining the kinetics of redox reaction and the diffusion of electrolyte ion on the surface of the electrode-electrolyte. With a higher slope linear at low frequency, the supercapacitor is more closer to the ideal capacitance and a better power characteristic of the electrode material (Wu et al., 2013). The frequency corresponding to the corner point between the semi-circle and the linear is called corner frequency, and the frequency value of this point reflects the rate of charge and discharge of the supercapacitor electrode materials (Taberna et al., 2006). It can be clearly seen that AAC has a larger diameter of the semicircle in high frequency region, leading to a larger ion charge transfer resistance. The charge transfer resistance of AAC is 0.6 Ω, yet only 0.2 Ω of MAC. At the maximum frequency point, the intersection of semicircle curve and abscissa coordinate (Z', Ohm) reflects the equivalent series resistance (ESR) of supercapacitor electrodes (Noorden et al.,

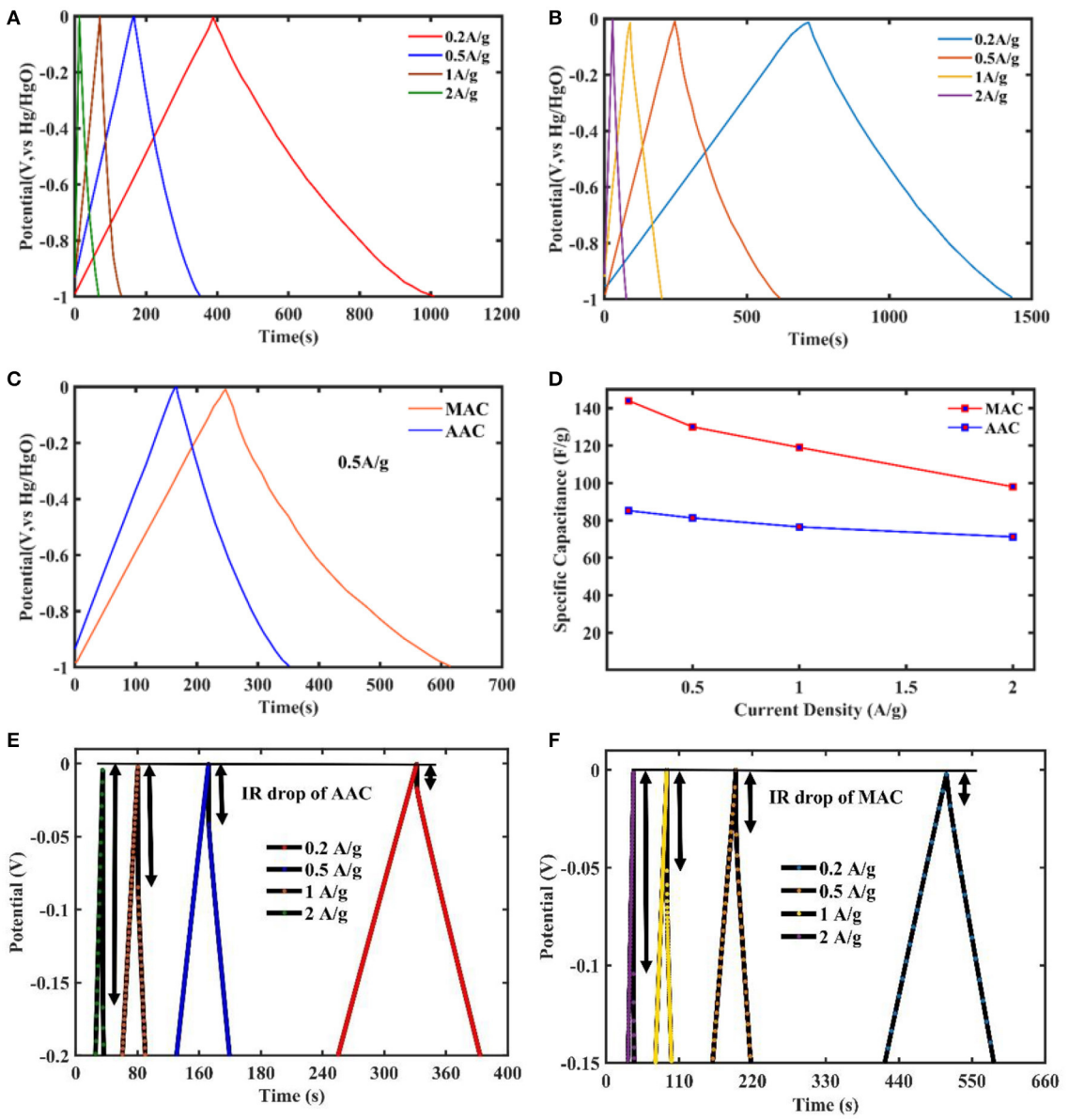

FIGURE 8 | (A) GCD lines of MAC obtained at 0.2, 0.5, 1, and 2 A/g; **(B)** GCD lines of AAC obtained at 0.2, 0.5, 1, and 2 A/g; **(C)** GCD lines of MAC and AAC obtained at 0.5 A/g; **(D)** Specific capacitance of MAC and AAC at different current density; **(E)** IR drop of AAC; **(F)** IR drop of MAC.

2012). The ESR of AAC reaches 0.28 Ω, over 7 times than the value of AAC (0.04 Ω). The above results show that MAC has abundant porosity which is more suitable for the diffusion of electrolyte ions, and the conclusion is mutually validated with results obtained from characterization experiments. In addition, the ESR is a vital factor for the specific power of supercapacitors, and a lower ESR value contributes to a higher specific power of MAC. The equivalent circuit of the electrode and solution is exhibited in the insert of **Figure 7** which includes C_d (double-layer capacitance), Z_w (Warburg impedance), R_{ct} (charge-transfer resistance) and R_s (spreading resistance).On the other hand, the curve of MAC in the low frequency region is more parallel to the "-Z" axis. The corner frequency of MAC electrode is significantly higher than AAC which can be clearly seen in the inset of **Figure 7**. Therefore, the electrodes of MAC supercapacitor can be charged and discharged at a higher rate. This result is in good agreement with the CV tests.

GCD Test

Galvanostatic charge-discharge (GCD) technique is often used in the test of battery, and it is also applied for investigating the electrochemical performance of supercapacitor electrodes (Tao et al., 2007). In the GCD test, the current density is a constant, and the voltage is the response signal changing with time. The first cycle curve of AAC and MAC in GCD tests of three electrodes system are described in **Figures 8A,B**. The electrolyte is still 2M KOH with the same potential window of −1 to 0 V at current densities of 0.2, 0.5, 1, and 2 A/g. All the curves show a good isosceles triangle shape, suggesting good

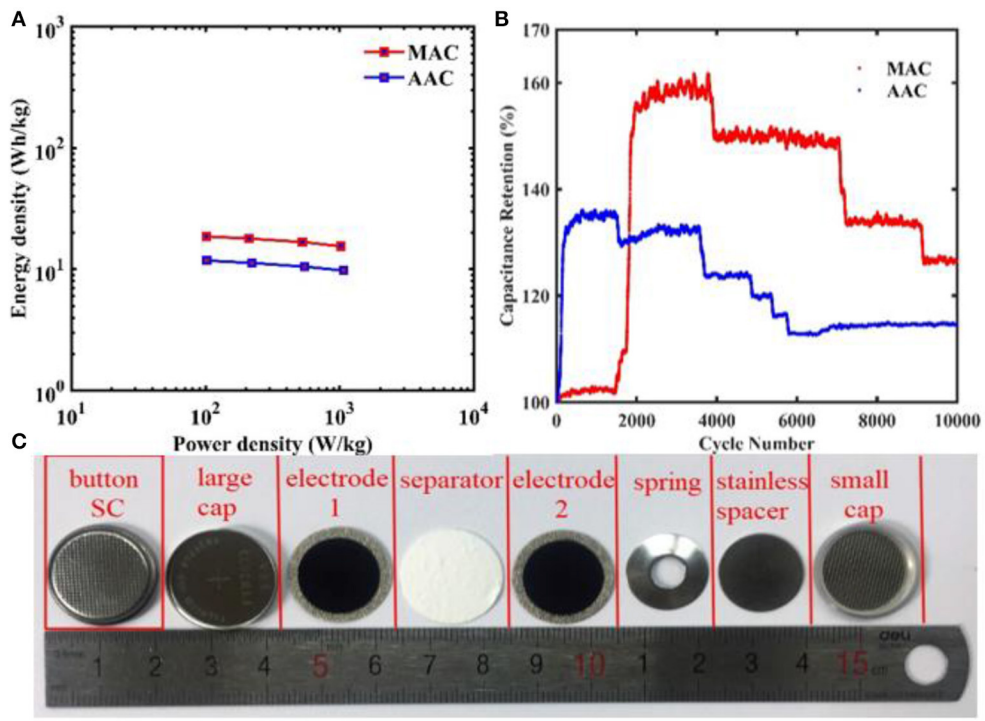

FIGURE 9 | (A) Ragone plots of MAC and AAC; **(B)** capacitance retention of MAC and AAC at the current density of 0.5 A/g; **(C)** button SC and primary structures.

TABLE 2 | Summary of electrochemical performances of biomass activated carbon.

Biomass precursor	Activation method	Current density A/g	Specific capacitance F/g	capacitance retention	References
Pomelo peel	C:KOH = 1:3	1	160	100% 10,000 cycles	Zhong-Yu et al., 2018
Infested ash tree	HNO_3	1	123	98% 1,500 cycles	Kouchachvili et al., 2015
Cladophora	6 M KOH	1	340	93.1% 10,000 cycles	Pourhosseini et al., 2018
Banana fiber	C:KOH = 1:5	0.5	66	70% 500 cycles	Subramanian et al., 2007
Konjac glucomannan	C:KOH = 1:3	1	273.8	96.3% 5,000 cycles	Li et al., 2018
Rice straw	4.3 M KOH	0.1	400	93.6% 10,000 cycles	Jin et al., 2018
Millet straw	C:KOH = 1:5	0.2	144	125% 10,000 cycles	This work

EDLC characteristics of two groups of electrodes. As can been also seen in **Figures 8A,B**, with the increase of current density, the specific capacitance of the two activated carbon electrodes decreases to a certain extent, and the charge-discharge time decreases greatly, which may be due to the increase of charge per unit time at high current density, resulting in the inadequate entry of electrolyte ions into porous carbon and occupying only a small part of the activity position. This conclusion can also be drawn from **Figures 8C,D**. The specific capacitance of supercapacitor based on MAC is calculated to 144 F/g at a current density of 0.2 A/g, while the value of AAC is only 85.2 F/g. However, with the increase of current density, the specific capacitance of MAC decreases faster. At 2 A/g, the specific capacitance of MAC decreases to 98 F/g with a reduction of 46 F/g, but AAC decreases by only 14 F/g. This result illustrates that MAC is more suitable for lower current density conditions than AAC. The instantaneous voltage drop (IR drop) reflects the combined ohmic resistance of electrodes, electrolyte and contact resistances (Yang et al., 2017). In order to clearly see IR drop of MAC and AAC at different current densities, the parts of **Figures 8A,B** has been redrawn in **Figures 8E,F** (−0.15 to 0.01 V and −0.2 to 0.01 V of Y-axis, respectively). The IR drop of MAC and AAC electrode system at 2 A/g are 0.16 and 0.10 V, respectively. At each current density, MAC is superior to AAC in IR drop which corresponds to the results of EIS test. This can be explained by microstructure in SEM images. Compared with AAC, MAC has a large number of tube structures which are helpful for the transfer of electrolyte ions and a reduction of diffusion resistance.

Based on the GCD test, the energy density and power density are obtained by Equations (9) and (10) at different densities and Ragone plots are shown in **Figure 9A**. It is apparent that MAC perform better than AAC. The maximum energy density of MAC reaches up to 18.67 W h/Kg at the power density of 101.35 W/Kg. The cycle life is also a significant requirement for supercapacitors (Balducci et al., 2017). In order to study the capacitance retention of MAC and AAC after multiple charging and discharging at the same current density, 100,000 cycles of continuous GCD test at 0.5 A/g were carried out by button symmetry SC which consists of large cap, electrode 1, separator, electrode 2, spring, stainless spacer and small cap as shown in **Figure 9C**. The capacitance retention rate of MAC and AAC symmetric button SCs is calculated by using the discharge capacitance of the first cycle as standard capacitance. The changes of capacitance retention rate are described in **Figure 9B**. What's interesting is that the capacitance retention rate of button SCs made of AAC and MAC rises abruptly at around the 100th and 2,000th cycles, respectively, and then presents a step-by-step decline because of the slightly rising temperature of SCs after a long time of constant current charging and discharging in the initial stage resulting in the acceleration of ions diffusion. After that, the structure of two electrode materials is destroyed by stages in constant cycles, so the capacitance retention rate shows a step-by-step decline (Teng et al., 2019). The capacitance retention of MAC button SC maintained at 125% after 9,000 cycles, and that of AAC button SC maintained at 114% after 7,000 cycles without subsequent changes. After 10,000 cycles of constant current charging and discharging, the capacitance retention of MAC is 11% higher than that of AAC. The coulombic efficiency of MAC and AAC remains 99.5 and 97.4%, respectively. The good cycling stability and coulombic efficiency of MAC is attributed to its rich tube structures and fish-scale-like inner surface by which electrolyte ions adsorb and desorb smoothly in each cycle of charging and discharging.

Our results were compared with some other references' biomass activated carbon in **Table 2**. Our MAC performs a good specific capacitance at 0.2 A/g with 144 F/g. What's more, the button symmetry SC made of MAC displays an excellent capacitance retention which is 125% after 10,000 cycles of constant current charging and discharging. The superior feature indicates that MAC is a promising electrode active material for supercapacitors.

CONCLUSIONS

In this study, two kinds of activated carbon were obtained by the same method of carbonizing and activating. The mass ratio was 5:1 (KOH: carbon) to activate millet straw and anthracite precursor carbon. The activated carbons show a large SSA ($S_{BET-MAC}$ = 1,264.8 m^2/g, $S_{BET-AAC}$ = 1,424.1 m^2/g) and hierarchical porosity. Although the SSA of MAC is smaller than AAC, the average pore size is larger (D_{ap-MAC} = 3.018 nm, D_{ap-AAC} = 2.169 nm), which is more conducive to a large specific capacitance and the diffusion of electrolyte ions. These views has been verified via CV and EIS tests, demonstrating a larger area of CV curve of MAC at each scan rate and a lower ESR of MAC ($R_{ESR-MAC)}$ = 0.043 Ω, $R_{ESR-AAC}$ = 0.28 Ω). Moreover, MAC shows a good capacitive behavior as the electrode material of supercapacitor with an excellent specific capacitance of 144 F/g at 0.2 A/g and a good retention rate of 125% after 10,000 cycles carried out button symmetry SCs for its rich tube structures and fish-scale-like inner surface. In conclusion, the millet straw activated carbon and anthracite activated carbon can be obtained by simple, environmental-friendly carbonizing and activating processes, and they both have a good performance of supercapacitors.

DATA AVAILABILITY STATEMENT

The datasets generated for this study are available on request to the corresponding author.

AUTHOR CONTRIBUTIONS

YD carried out the work. TW and DD helped in manuscript preparation. TW and YZ supervised the work.

FUNDING

This work was supported by National Natural Science Foundation of China (grant no. 51706069).

REFERENCES

Akash, B. A., and O'Brien, W. S. (2015). The production of activated carbon from a bituminous coal. *Int. J. Energy Res.* 20, 913–922. doi: 10.1002/(SICI)1099-114X(199610)20:10<913::AID-ER205>3.0.CO;2-7

Balducci, A., Belanger, D., Brousse, T., Long, J. W., and Sugimoto, W. (2017). Perspective—a guideline for reporting performance metrics with electrochemical capacitors: from electrode materials to full devices. *J. Electrochem. Soc.* 164, A1487–A1488. doi: 10.1149/2.0851707jes

Dai, C., Wan, J., Shao, J., and Ma, F. (2017). Hollow activated carbon with unique through-pore structure derived from reed straw for high-performance supercapacitors. *Mater. Lett.* 193, 279–282. doi: 10.1016/j.matlet.2017.02.007

Frackowiak, E., and Béguin, F. (2002). Electrochemical storage of energy in carbon nanotubes and nanostructured carbons. *Carbon* 40, 1775–1787. doi: 10.1016/S0008-6223(02)00045-3

Genovese, M., and Lian, K. (2017). Polyoxometalate modified pine cone biochar carbon for supercapacitor electrodes. *J. Mater. Chem.* A 5, 3939–3947. doi: 10.1039/C6TA10382K

Grahame, D. C (1947). The electrical double layer and the theory of electrocapillarity. *Chem. Rev.* 41, 441–501. doi: 10.1021/cr60130a002

Guo, F., Jia, X., Liang, S., Jiang, X., Peng, K., and Qian, L. (2019). Design and synthesis of highly porous activated carbons from Sargassum as advanced electrode materials for supercapacitors. *J. Electrochem. Soc.* 166, A3109–A3118. doi: 10.1149/2.0191914jes

He, X., Li, R., Qiu, J., Xie, K., Ling, P., Yu, M., et al. (2012). Synthesis of mesoporous carbons for supercapacitors from coal tar pitch by coupling microwave-assisted KOH activation with a MgO template. *Carbon* 50, 4911–4921. doi: 10.1016/j.carbon.2012.06.020

Ji, H., Zhao, X., Qiao, Z., Jung, J., Zhu, Y., Lu, Y., et al. (2014). Capacitance of carbon-based electrical double-layer capacitors. *Nat. Commun.* 5:3317. doi: 10.1038/ncomms4317

Jin, H., Hu, J., Wu, S., Wang, X., Zhang, H., Xu, H., et al. (2018). Three-dimensional interconnected porous graphitic carbon derived from rice straw for high performance supercapacitors. *J. Power Sources* 384, 270–277. doi: 10.1016/j.jpowsour.2018.02.089

Kouchachvili, L., Maffei, N., and Entchev, E. (2015). Infested ash trees as a carbon source for supercapacitor electrodes. *J. Porous Mater.* 22, 979–988. doi: 10.1007/s10934-015-9972-2

Li, Q., Bai, X., Meng, Q., Chen, T., Zhu, W., Yao, W., et al. (2018). Porous biochar generated from natural *Amorphophallus konjac* for high performance supercapacitors. *Appl. Surf. Sci.* 448, 16–22. doi: 10.1016/j.apsusc.2018.04.086

Liu, D., Zhang, W., Lin, H., Li, Y., Lu, H., and Wang, Y. (2015). Hierarchical porous carbon based on the self-templating structure of rice husk for high-performance supercapacitors. *RSC Adv.* 5, 19294–19300. doi: 10.1039/C4RA15111A

Lozano-Castelló, D., Calo, J. M., Cazorla-Amorós, D., and Linares-Solano, A. (2007). Carbon activation with KOH as explored by temperature programmed techniques, and the effects of hydrogen. *Carbon* 45, 2529–2536. doi: 10.1016/j.carbon.2007.08.021

Naderi, H. R., Norouzi, P., and Ganjali, M. R. (2016). Electrochemical study of a novel high performance supercapacitor based on MnO_2/nitrogen-doped graphene nanocomposite. *Appl. Surf. Sci.* 366, 552–560. doi: 10.1016/j.apsusc.2016.01.058

Noorden, Z. A., Sugawara, S., and Matsumoto, S. (2012). Electrical properties of hydrocarbon-derived electrolytes for supercapacitors. *IEEJ Trans. Electr. Electron. Eng.* 7, S25–S31. doi: 10.1002/tee.21802

Pandolfo, A. G., and Hollenkamp, A. F. (2006). Carbon properties and their role in supercapacitors. *J. Power Sources* 157, 11–27. doi: 10.1016/j.jpowsour.2006.02.065

Pourhosseini, S. E. M., Norouzi, O., Salimi, P., and Naderi, H. R. (2018). Synthesis of a novel interconnected 3D pore network Algal Biochar constituting iron nanoparticles derived from a harmful marine biomass as high-performance asymmetric supercapacitor electrodes. *ACS Sust. Chem. Eng.* 6, 4746–4758. doi: 10.1021/acssuschemeng.7b03871

Qiu, Z., Wang, Y., Bi, X., Zhou, T., Zhou, J., Zhao, J., et al. (2018). Biochar-based carbons with hierarchical micro-meso-macro porosity for high rate and long cycle life supercapacitors. *J. Power Sources* 376, 82–90. doi: 10.1016/j.jpowsour.2017.11.077

Rose, M., Korenblit, Y., Kockrick, E., Borchardt, L., Oschatz, M., Kaskel, S., et al. (2011). Hierarchical micro- and mesoporous carbide-derived carbon as a high-performance electrode material in supercapacitors. *Small* 7, 1108–1117. doi: 10.1002/smll.201001898

Saliger, R., Fischer, U., Herta, C., and Fricke, J. (1998). High surface area carbon aerogels for supercapacitors. *J. Non Cryst. Solids* 225, 81–85. doi: 10.1016/S0022-3093(98)00104-5

Subramanian, V., Luo, C., Stephan, A. M., Nahm, K. S., Thomas, S., and Wei, B. (2007). Supercapacitors from activated carbon derived from banana fibers. *J. Phys. Chem. C* 111, 7527–7531. doi: 10.1021/jp067009t

Taberna, P. L., Portet, C., and Simon, P. (2006). Electrode surface treatment and electrochemical impedance spectroscopy study on carbon/carbon supercapacitors. *Appl. Phys. A* 82, 639–646. doi: 10.1007/s00339-005-3404-0

Tao, F., Zhao, Y., Zhang, G., and Li, H. L. (2007). Electrochemical characterization on cobalt sulfide for electrochemical supercapacitors. *Electrochem. Commun.* 9, 1282–1287. doi: 10.1016/j.elecom.2006.11.022

Teng, Z., Han, K., Li, J., Gao, Y., Li, M., and Ji, T. (2019). Ultrasonic-assisted preparation and characterization of hierarchical porous carbon derived from garlic peel for high-performance supercapacitors. *Ultrasonics Sonochem.* 60, 104756. doi: 10.1016/j.ultsonch.2019.104756

Tian, W., Gao, Q., Tan, Y., Yang, K., Zhu, L., Yang, C., et al. (2015). Bio-inspired beehive-like hierarchical nanoporous carbon derived from bamboo-based industrial by-product as a high performance supercapacitor electrode material. *J. Mater. Chem. A* 3, 5656–5664. doi: 10.1039/C4TA06620K

Wang, J., and Kaskel, S. (2012). KOH activation of carbon-based materials for energy storage. *J. Mater. Chem.* 22:23710. doi: 10.1039/c2jm34066f

Wu, T. H., Chu, Y. H., Hu, C. C., and Hardwick, L. J. (2013). Criteria appointing the highest acceptable cell voltage of asymmetric supercapacitors. *Electrochem. Commun.* 27, 81–84. doi: 10.1016/j.elecom.2012.10.033

Xu, Y., Lin, Z., Huang, X., Wang, Y., Huang, Y., and Duan, X. (2013). Functionalized graphene hydrogel-based high-performance supercapacitors. *Adv. Mater.* 25, 5779–5784. doi: 10.1002/adma.201301928

Yamashita, Y., and Ouchi, K. (1982). Influence of alkali on the carbonization process—III: dependence on type of alkali and of alkali earth compounds. *Carbon* 20, 55–58. doi: 10.1016/0008-6223(82)90074-4

Yang, K., Cho, K., Yoon, D. S., and Kim, S. (2017). Bendable solid-state supercapacitors with Au nanoparticle-embedded graphene hydrogel films. *Sci. Rep.* 7:40163. doi: 10.1038/srep40163

Yoo, J. J., Balakrishnan, K., Huang, J., Meunier, V., Sumpter, B. G., Srivastava, A., et al. J., et al. (2011). Ultrathin planar graphene supercapacitors. *Nano Lett.* 11, 1423–1427. doi: 10.1021/nl200225j

Zhong-Yu, W., Lei, F., You-Rong, T., Wei, W., Xing-Cai, W., and Jian-Wei, Z. (2018). Pomelo Peel derived hierarchical porous carbon as electrode materials for high-performance supercapacitor. *Chin. J. Inorg. Chem.* 34, 1249–1260. doi: 10.11862/CJIC.2018.166

Conflict of Interest: The authors declare that the research was conducted in the absence of any commercial or financial relationships that could be construed as a potential conflict of interest.